Preprints of the 21st IFAC World Congress (Virtual)
Berlin, Germany, July 12-17, 2020

Two Camera 3D Time Series Reconstruction of a Mesh Subjected to Differential Excitation

Michael Joon Seng Goh, Yeong Shiong Chiew, Ji Jinn Foo

Monash University Malaysia, Selangor, Malaysia
(e-mail: Michael.Goh@monash.edu, Chiew.Yeong.Shiong@monash.edu, Foo.Ji.Jinn@monash.edu).

Abstract: The present study proposes a novel bio-inspired scheme for the 3D time series reconstruction of a Mesh. The key motivation of this study is to develop a cost effective and accessible system without compromising capabilities for the fundamental understanding in complicated external stimuli-induced vibration of a Mesh. A bio-inspired algorithm traces along the strands of the mesh to match a known control point to the next keypoint until the entire surface is matched for the critical reconstruction at the first frame/timestep. The match is then disseminated to the subsequent frames steps via digital image correlation and photogrammetric methods applied to effectively recover the time series response of the dynamic surface. This study offers significant and quantitative insight into the vibration and fluctuation of the entire excited surface. A 160mm×160mm mesh fluctuation is successfully re-constructing with a sampling density of approximately 1600 points at 24 frames per second. The proof-of-concept experiment was able to detect the undulation of mesh under an in-phase and an out-of-phase excitation, which result in the reconstruction of the point cloud with a 0.38mm error, as well as the frequency and phase angle accuracy attainments of about 99.1% and 86.0%, respectively. In short, the current reconstruction scheme may provide insights into the control and response of a piezoelectric mesh.

Keywords: Process control applications; Measurement and instrumentation; Advanced control technology

1. INTRODUCTION

Vibrations have a ubiquitous existence, permeating into every aspect of life with significance in acoustics, structures, electronics, transportation, energy harvesting and cell biology (Ahmed et al., 2011, Kulkarni et al., 1996, Bandhu et al., 2004, Ruggles, 1969, Goh et al., 2020). One such application that sparked our interest is the recent development of piezoelectric generators in strand form (Sim et al., 2015, Wang and Song, 2006) which could potentially be integrated into fabrics, or woven into Meshes. Possible practical application of such a composite include the integration of piezoelectric material into clothing to power wearable electronics, canvas canopies and tents for energy harvesting, wire fences for energy harvesting and sensing, or the use of piezoelectric Meshes as direct wind energy harvesters, which could potentially be a scalable, passive small footprint generator for harsh environments or confined spaces. As both the excitation frequency and resonant frequency are key to determining the eventual efficiency (Kim et al., 2011, Cho et al., 2006), it is essential to be able to study the basis fluctuations and vibration of the generator for tuning and optimization. Furthermore, the piezoelectric mesh could potentially be used to modify fluid flow in a channel by acting as an excitation device. To this end, a system capable of time series reconstruction of a Mesh is to be developed as a prerequisite to further study the potential application of a piezoelectric Mesh as a sensor or use as an excitation device. This is essential as the electrical signal to/from the mesh needs to be correlated to the physical response of the mesh. In this paper, we propose a unique approach inspired by how humans intuitively determine salient features of Meshes, match these features between stereo pairs as well as images at subsequent time steps as shown in Fig. 1 where the left and right view are matched in t_0 after which the matching can be shared to t_1 until t_n.

Photogrammetric methods present a unique attraction as it permits non-contact full field measurements (Yue et al., 2010, Ryall and Fraser, 2002, Lilienblum and Al-Hamadi, 2015). Modern photogrammetric methods such as (Kuhn et al., 2017, Vu et al., 2012, Zhu and Gao, 2010) and (Furukawa and Ponce, 2010) can provide the high accuracy, high resolution reconstruction necessary to study the subtle vibrations and fluctuations. As these methods require multiple views, it is more suited for applications to static subjects where typically a single camera is moved to record the subject from multiple views or mirrors are used. Adapting these methods to dynamic study would require a significant number of synchronized cameras to be employed. Several high accuracy approaches that use structured light, dot projection or attached markers have also been used for dynamic study (Lee and Rhee, 2013, Pappa et al., 2003, Ryall and Fraser, 2002). However, due to the tradeoff between spatial reconstruction resolution and equipment cost as multiple cameras are needed, these approaches may be inaccessible to certain research groups. Furthermore, structured light and dot projection setup may require long exposure time for high spatial resolution, limiting it's used for high speed dynamic investigations. The use of retroreflective markers allows for better sampling rates to be achieved but may sacrifice the spatial resolution due to the physical size of the markers. The markers may also be

unsuitable for some applications where attachment of the marker to the object will alter the object's response. Stereoscopic methods such as those reviewed in (Scharstein and Szeliski, 2002) needing as little as two cameras generally estimate a disparity map which focuses more on distinguishing planes at different depth; these methods are not commonly optimized for a high level of surface detail required for the current vibrational study (Pachidis and Lygouras, 2007).

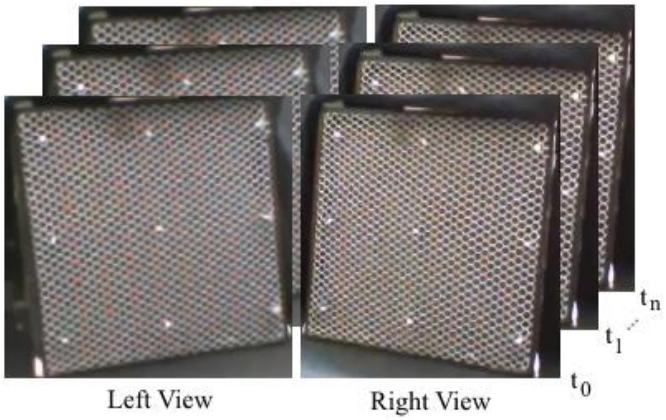

Fig. 1 Example of left and right view at multiple timesteps.

Most stereoscopic methods utilise some form of stereomatching algorithm to obtain the disparity map or perform the 3D reconstruction of the object. Stereomatching is in essence matching parts of an image to its corresponding parts in the image taken from the complementary camera. In its simplest form, this is accomplished via comparing the intensity values; finding the smallest sum of absolute difference (SAD) or sum of squared difference (SSD) between pixels of a reference window on one image to that of its complementary image (Scharstein and Szeliski, 2002, Shimizu and Okutomi, 2005, Xue et al., 2014). Features such as SIFT (Lowe, 1999), SURF (Bay et al., 2008), and FREAK (Alahi et al., 2012) encode a large amount of information about a point and its neighbourhood allowing for more confidence in the matchings performed. Yet, when faced with objects or scenes with repetitive patterns, there is a tendency for false correspondence to occur owing to confusion (Barrois et al., 2010). Methods such as (Royer et al., 2017, Zhao et al., 2011) handle confusing scenes by identifying and eliminating confusing points; however this may lead to crucial data being lost especially if the object is composed mainly of repetitive patterns.

To study the dynamic behaviour of the object, digital image correlation (DIC) can be applied; such as in the work by (Lavatelli and Zappa, 2016) to study cantilever beam vibration. (Lavatelli and Zappa, 2017) also presented advance DIC methods able to cope with motion blur; essential for study of high speed motions using cameras.

2. WORKING PRINCIPLE

We have identified three main steps required for the time series reconstruction of Meshes. These are i) keypoint extraction, ii) stereo matching and iii) static-to-transient matching as shown in Fig.2. The overall process is detailed in Sections 2.1, 2.2 and 2.3.

2.1. Keypoint Extraction

The first step is identifying keypoints on the Mesh to be used for stereo matching. This is important as it reduces the computational load of the reconstruction by significantly reducing the number of inputs into the stereomatching. However, the keypoints must still be able to provide an accurate reconstruction of the Mesh with sufficient detail. Drawing inspiration from how humans view the intersection of Meshes as salient features, we propose the use of these Mesh intersections as the keypoints. Fig. 3 shows a sample of a Mesh with the intersections highlighted in yellow and the desired keypoints to be extracted as red "X"s.

In order to ensure that the majority of the intersections are captured with minimal false positives and false negatives during keypoint extraction, the appropriate scale needs to be determined. This scale will be used to determine the minimum spacing between keypoints as well as the position of the keypoint within the intersection. As Meshes are by definition and design repetitive structures, a single scale can be applied to each study.

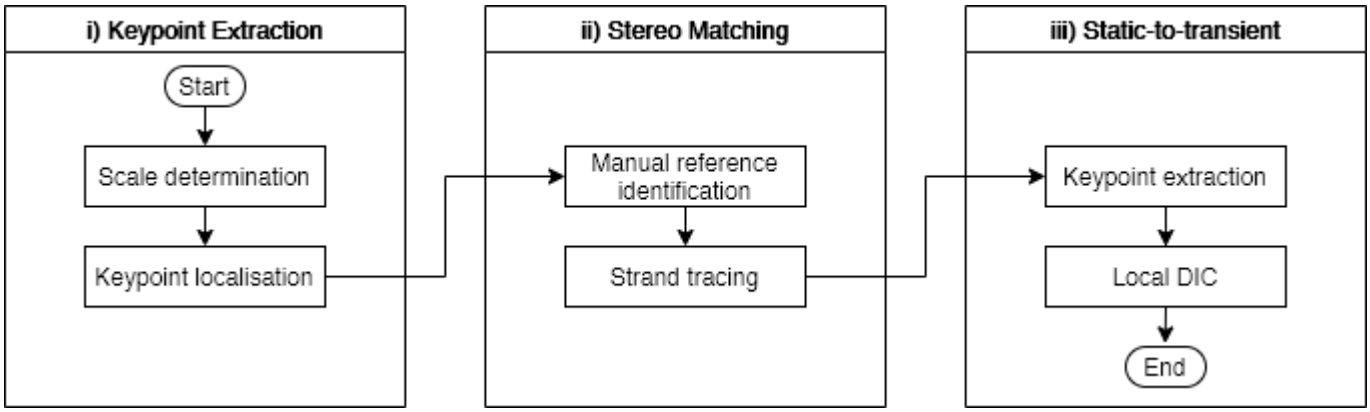

Fig. 2 Overview of the proposed 3D time series reconstruction of nets or meshes.

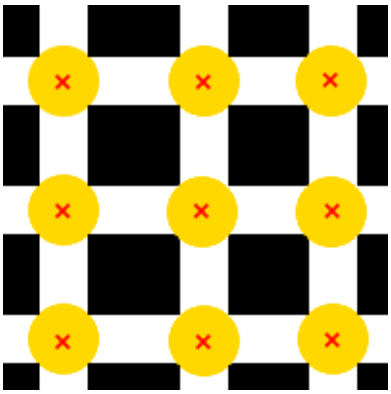

Fig. 3 Example of a net (white) with intersections highlighted in yellow and centres of intersections marked with a red "X"

As for the localization of the keypoints, ideally each intersection should have a single keypoint. This is achieved by looking for the pixel in each intersection that has the most Mesh pixels around it. This can be expressed as in Eq.1 below where the centre is the pixel with the largest ratio, $Pixel_{Ratio}$ in each intersection.

$$Pixel_{Ratio} = \frac{\sum_{x=-w}^{w}\sum_{y=-h}^{h} \mathrm{IsMesh(x,y)}}{4wh} \quad (1)$$

Where *IsMesh(x,y)* is a function which returns 1 if the pixel at position *(x,y)* is on the Mesh, *w* is width of the intersection and *h* is the height of the intersection

2.2. Stereo Match

Once the keypoints have been extracted, the correspondence between the keypoints in the left view and the right view needs to be determined in order for each intersection to be triangulated and the Mesh reconstructed.

Drawing inspiration from how humans intuitively approach the problem when presented with the task of manually performing the stereo matching; we have developed the following scheme. Starting from a known match, tracing the Mesh along its strand to the next keypoint for both left and right view returns another correct match. We can then continue trancing along the strand to obtain the next match and keep repeating this for all subsequent keypoints. An example of this tracing procedure can be seen in Fig. 4 where the green arrows show a trace along the bottom of the Mesh while the yellow and blue arrows show two possible paths the trace can continue.

The tracing is achieved by ensuring that θ as defined in Eq. 2 below is the same or very close for both the left and right view.

$$\theta = atan2\left(\frac{Y_n - Y_{n-1}}{X_n - X_{n-1}}\right) - atan2\left(\frac{Y_n - Y_{n+1}}{X_n - X_{n+1}}\right) \quad (2)$$

Where n is the number of points matched, X_n is the x-axis coordinate of the nth matched point and Y_n is the y-axis coordinate of the nth matched point. Also note that the $n+1$ point refers to the new keypoint considered for tracing and matching.

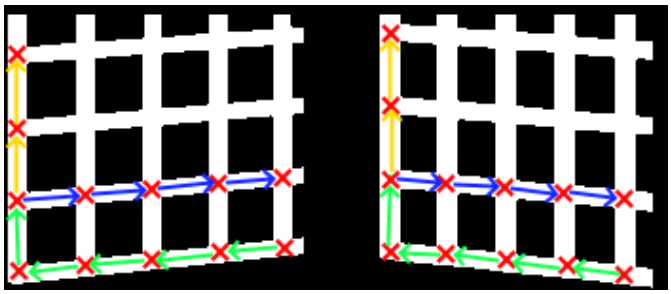

Fig. 4 Example of left view (left) and right view (right) of a net with visualization of tracing algorithm as green, yellow and blue arrows.

2.3. Static-to-transient Matching

Although the process described in Sections 2.1 and 2.2 can be applied to every time step, we drew inspiration from humans once again and found that it is more efficient to match the keypoints from each view to keypoints from subsequent timesteps of the same view. This is more efficient as opposed to performing stereo matching for each time step as the changes between each timestep is a lot less significant than the visual difference between the left and right views due to perspective distortions. For small inter-timestep deformation of the Mesh where the camera framerate is high relative to the rate of the Mesh's deformation, each keypoints can be simply matched by finding the nearest keypoint in the previous timestep. However, if the inter-timestep deformation is large, local digital image correlation (DIC) will need to be applied at the right scale to ensure each keypoint is correctly matched to its corresponding keypoint from the previous timestep. The local DIC is implemented by using a window around the keypoint in the previous timestep as the reference to perform the 2D discrete cross correlation which will yield the corresponding keypoint location in the current timestep.

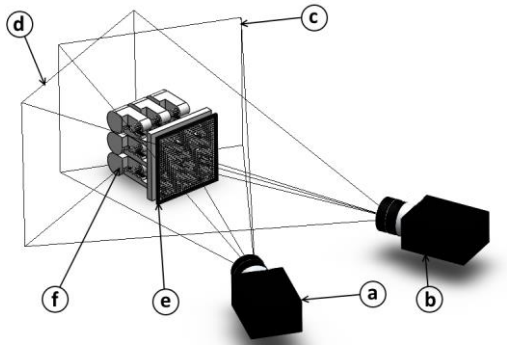

Fig. 5 Schematic of experiment setup: Cameras (a and b), the image planes (c and d), the mesh (e) and actuators (f)

3. EXPERIMENTAL SETUP USING HEXAGONAL CELL MESH

As a proof of concept, we have applied the reconstruction scheme presented in Section 2 to the time series reconstruction of a mesh under two excitation conditions. The experimental setup is as in Fig. 5 with 2 USB cameras used to capture the stereo image time series. A 160mm×160mm

hexagonal cell mesh is attached at 9 points to linear actuators as shown in Fig. 5. Each linear actuator is controlled independently to impart 2 different forms of excitation, either In-phase excitation or an Out-of-phase excitation. In both scenarios, the actuators impart a sinusoidal excitation with a period of 0.55s or 1.818Hz.

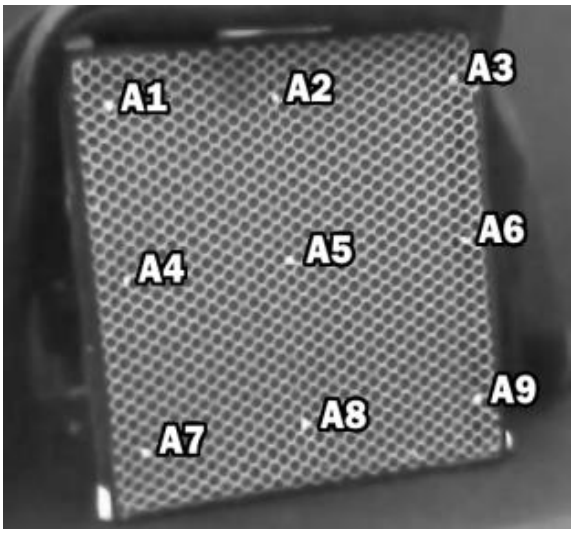

Fig. 6 The hexagonal cell mesh with notation A1 to A9 indicating the position the actuators are attached to the mesh.

Applying the presented keypoint extraction and stereomatching methodto the first frame/ timestep, 1620 keypoints were successfully matched and the mesh reconstructed in 3D. DIC is then applied to subsequent frames to obtain the 3D time series topology of the mesh.

3.1. In-Phase Excitation

For the in-phase excitation, all nine actuators were triggered simultaneously to ensure the sinusoidal excitation at all nine points of the mesh were in-phase. As shown in Fig. 7a, 6b, 6c, and 6d, it is seen that the mesh was pushed from its initial position to its maximum convexity before returning to its initial position. Fig. 7a shows the net moving rightwards in the left camera's view (magnified for clarity) which indicates a positive Z-axis motion. Conversely, Fig. 7d shows a leftward motion indicating a negative Z-axis motion. The Mesh's motion at the interface to actuators *A8* and *A5* are quantified by plotting the time series Z-axis position of points *P1* and *P2* respectively in Fig. 7e. We are able to fit sinusoidal waves to the time series data where both waveforms were found to have a frequency of 1.7964Hz, which is close to the actuator's input waveform of 1.8182Hz. Note that the regions highlighted as *I, II, III* and *IV* in Fig. 7e corresponds to Fig. 7a, Fig. 7b, Fig. 7c and Fig. 7d respectively. It can also be observed that there is no noticeable phase difference between the two waveforms as the actuators were triggered simultaneously. The amplitude distribution (Fig. 7e) shows that the rigid connection between the mesh and the actuator has higher amplitude as compared to the mesh around each actuator as expected. Furthermore, as seen in Fig. 7f, the areas near the edge display rather low amplitude as expected, due to the stationery plastic frame limiting the mesh fluctuation. As for the phase across the mesh, Fig. 7g illustrates the phase angle distribution where the distribution is almost uniform as the actuators were triggered simultaneously.

3.2. Out-of-Phase Excitation

Looking into the triggering sequence of the out-of-phase excitation, the first set of actuators (A3, A6 and A9) were triggered together to move outwards (positive Z direction). After a 185ms delay the second set was triggered with the A2 and A8 moving outward while the A5 moved inwards. After which the third set (A1, A4 and A7) was triggered to move outwards 185ms after the second set. Based on Fig. 8a to Fig. 8d, we can observe that each set of actuators act in unison while remaining at a different phase to other sets. This is observed as similar Z-axis displacements within sets of actuators. Looking at the time series of P1 and P2 (Fig. 8e), we were able to fit two sinusoidal waveforms of 1.8018Hz which are close to the actuating 1.8182Hz. A detected phase difference of 0.86π between P1 and P2 does not differ too much from the expected phase difference of π. This error may be due to faults in the actuator triggering or video capturing and compression. The amplitude distribution (Fig. 8f) provides interesting insight as we can observe a significant overall lower amplitude in regions between the actuation points as compared to Fig. 7f, where the actuators were triggered in-phase. This may be due the regions between the actuation points experiencing a force opposing its direction of motion from the antagonistic actuators before reaching the same displacement as the actuating points. It could also be due to destructive interference of the excitation due to the out-of-phase actuators. The phase distribution intensity plot (Fig. 8g) further illustrates the phase difference as expected where there is a large phase difference between A5 with the rest of the surface, while the right side is also out of phase from the left by about 0.64π.

4. CONCLUSION

We have demonstrated a novel approach developed for the dynamic behavior study of a continuous surface. As a proof-of-concept, the presented scheme was applied to study the dynamic motion of a mesh under two different excitations; an in-phase and an out-of-phase excitation applied to nine points on the mesh. The scheme displayed promising sensitivity in detecting phase differences while attaining an accuracy of 86.0%. In addition, the fluctuation frequency was able to be detected with an accuracy of 99.1%. Although still in its infancy the proposed method presents a unique attraction in it being able to reconstruct the traditionally difficult mesh structure using only 2 cameras. We believe that this scheme will also be able to play a role in uncovering previously illusive details when paired with better cameras. We see great potential of this enabling technology in providing new insight into existing research and allowing a wider audience of researchers the opportunity to study the transient response of dynamic surfaces.

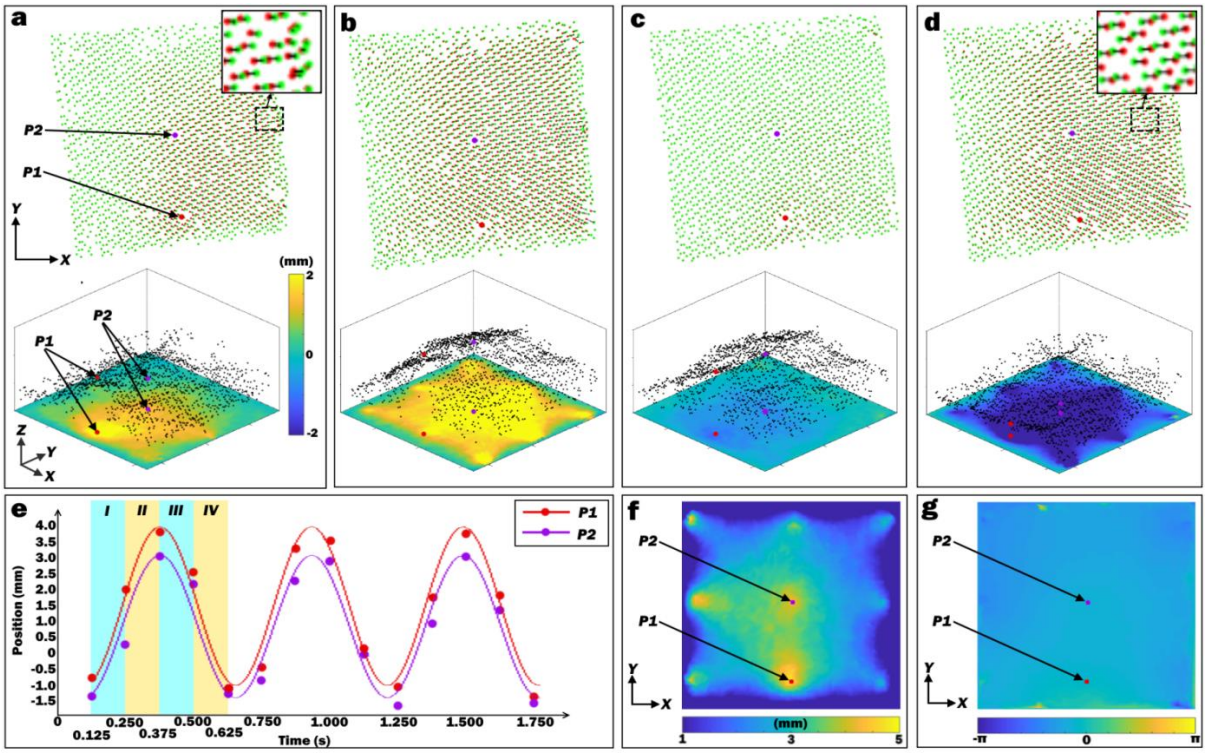

Fig. 7 Response of mesh to in-phase excitation. The top portion shows the position of the features in the left view (camera) for the current frame (t = 0.250s) in red and the previous frame (t = 0.125s) in green with the displacement marked by a black line. The portion below shows the reconstructed point cloud for the current frame with the intensity plot depicting the Z-axis movement relative to the previous frame. (b to d) are produced in the same way as (a) for frames t = 0.150s to t = 0.375s, t = 0.375s to t = 0.500s and t = 0.500s to t = 0.625s, respectively. (e) Time series Z-axis position of P1 and P2 plotted as dots with superimposed sinusoid with frequency calculated from the Fourier transform of the time series and amplitude corresponding to half the distance between the recorded maximum and minimum. (f) Z-axis amplitude distribution across the mesh visualized as intensity plot. (g) Phase angle distribution across the mesh visualized as intensity plot.

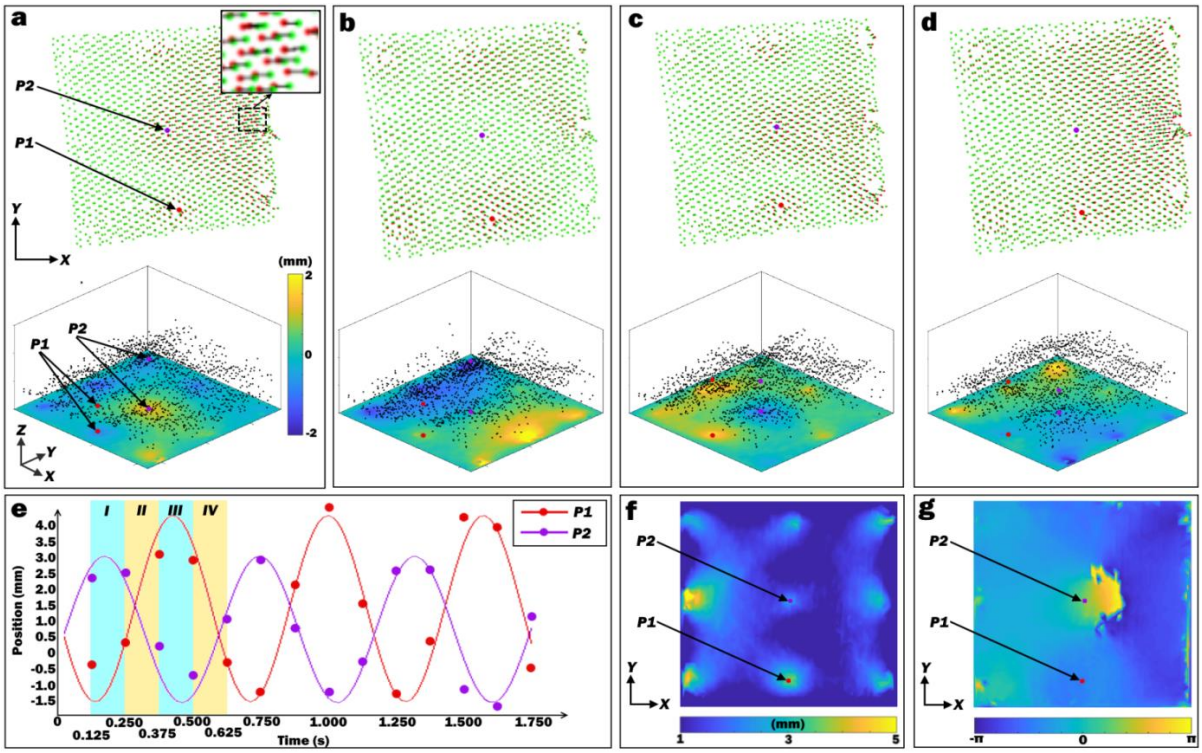

Fig. 8 Response of mesh to out-of-phase excitation. (a to d) Visualization of first 0.625 seconds. (e) Sinusoid fit to time series Z-axis position of P1 and P2. The amplitude (f) and phase angle (g) distributions.

ACKNOWLEDGMENT

The authors would like to thank the Malaysia Ministry of Higher Education (MOHE) for the financial support of the present research project (Project Code: FRGS/1/2014/TK01/MUSM/02/2). The authors would also like to thank Monash University Malaysia (MUM) for the financial support of the research project (MUM-24714739).

REFERENCES

AHMED, H. E. U., BANAN, R., ZU, J. W. & BAZYLAK, A. 2011. Free vibration analysis of a polymer electrolyte membrane fuel cell. *Journal of Power Sources,* 196**,** 5520-5525.

ALAHI, A., ORTIZ, R. & VANDERGHEYNST, P. 2012. FREAK: Fast Retina Keypoint.

BANDHU, R. S., ZHANG, X., SOORYAKUMAR, R. & BUSSMANN, K. 2004. Acoustic vibrations in free-standing double layer membranes. *Physical Review B,* 70**,** 4.

BARROIS, B., KONRAD, M., WÖHLER, C. & GROß, H.-M. 2010. Resolving stereo matching errors due to repetitive structures using model information. *Pattern Recognition Letters,* 31**,** 1683-1692.

BAY, H., ESS, A., TUYTELAARS, T. & VAN GOOL, L. 2008. Speeded-Up Robust Features (SURF). *Computer Vision and Image Understanding,* 110**,** 346-359.

CHO, J. H., RICHARDS, R. F., BAHR, D. F., RICHARDS, C. D. & ANDERSON, M. J. 2006. Efficiency of energy conversion by piezoelectrics. *Applied Physics Letters,* 89**,** 3.

FURUKAWA, Y. & PONCE, J. 2010. Accurate, Dense, and Robust Multiview Stereopsis. *Ieee Transactions on Pattern Analysis and Machine Intelligence,* 32**,** 1362-1376.

GOH, M. J. S., CHIEW, Y. S. & FOO, J. J. 2020. A Method for 3D Reconstruction of Net Undulation for Fluid Structure Interaction of Fractal Induced Turbulence. *IEEE Sensors Journal***,** 1-1.

KIM, H. S., KIM, J. H. & KIM, J. 2011. A Review of Piezoelectric Energy Harvesting Based on Vibration. *International Journal of Precision Engineering and Manufacturing,* 12**,** 1129-1141.

KUHN, A., HIRSCHMULLER, H., SCHARSTEIN, D. & MAYER, H. 2017. A TV Prior for High-Quality Scalable Multi-View Stereo Reconstruction. *International Journal of Computer Vision,* 124**,** 2-17.

KULKARNI, S., LEPPINGTON, F. G. & BROADBENT, E. G. 1996. Vibrations in three interconnected regions: Membranes or acoustic cells. *Proceedings of the Royal Society a:Mathematical Physical and Engineering Sciences,* 452**,** 1827-1844.

LAVATELLI, A. & ZAPPA, E. 2016. Modeling Uncertainty for a Vision System Applied to Vibration Measurements. *IEEE Transactions on Instrumentation and Measurement,* 65**,** 1818-1826.

LAVATELLI, A. & ZAPPA, E. 2017. A Displacement Uncertainty Model for 2-D DIC Measurement Under Motion Blur Conditions. *IEEE Transactions on Instrumentation and Measurement,* 66**,** 451-459.

LEE, H. & RHEE, H. 2013. 3-D measurement of structural vibration using digital close-range photogrammetry. *Sensors and Actuators a-Physical,* 196**,** 63-69.

LILIENBLUM, E. & AL-HAMADI, A. 2015. A Structured Light Approach for 3-D Surface Reconstruction With a Stereo Line-Scan System. *IEEE Transactions on Instrumentation and Measurement,* 64**,** 1258-1266.

LOWE, D. G. 1999. Object recognition from local scale-invariant features.

PACHIDIS, T. P. & LYGOURAS, J. N. 2007. Pseudostereo-Vision System: A Monocular Stereo-Vision System as a Sensor for Real-Time Robot Applications. *IEEE Transactions on Instrumentation and Measurement,* 56**,** 2547-2560.

PAPPA, R. S., BLACK, J. T., BLANDINO, J. R., JONES, T. W., DANEHY, P. M. & DORRINGTON, A. A. 2003. Dot-projection photogrammetry and videogrammetry of gossamer space structures. *Journal of Spacecraft and Rockets,* 40**,** 858-867.

ROYER, E., LELORE, T. & BOUCHARA, F. 2017. COnfusion REduction (CORE) algorithm for local descriptors, floating-point and binary cases. *Computer Vision and Image Understanding,* 158**,** 115-125.

RUGGLES, M. 1969. STEREOMICROGRAPHY USING THE BINOCULAR MICROSCOPE *. *Studies in Conservation,* 14**,** 31-35.

RYALL, T. G. & FRASER, C. S. 2002. Determination of structural modes of vibration using digital photogrammetry. *Journal of Aircraft,* 39**,** 114-119.

SCHARSTEIN, D. & SZELISKI, R. 2002. A taxonomy and evaluation of dense two-frame stereo correspondence algorithms. *International Journal of Computer Vision,* 47**,** 7-42.

SHIMIZU, M. & OKUTOMI, M. 2005. Sub-Pixel Estimation Error Cancellation on Area-Based Matching. *International Journal of Computer Vision,* 63**,** 207-224.

SIM, H. J., CHOI, C., LEE, C. J., KIM, Y. T., SPINKS, G. M., LIMA, M. D., BAUGHMAN, R. H. & KIM, S. J. 2015. Flexible, Stretchable and Weavable Piezoelectric Fiber. *Advanced Engineering Materials,* 17**,** 1270-1275.

VU, H. H., LABATUT, P., PONS, J. P. & KERIVEN, R. 2012. High Accuracy and Visibility-Consistent Dense Multiview Stereo. *Ieee Transactions on Pattern Analysis and Machine Intelligence,* 34**,** 889-901.

WANG, Z. L. & SONG, J. H. 2006. Piezoelectric nanogenerators based on zinc oxide nanowire arrays. *Science,* 312**,** 242-246.

XUE, T., QU, L. & WU, B. 2014. Matching and 3-D Reconstruction of Multibubbles Based on Virtual Stereo Vision. *IEEE Transactions on Instrumentation and Measurement,* 63**,** 1639-1647.

YUE, K. D., LI, Z. K., ZHANG, M. & CHEN, S. 2010. Transient full-field vibration measurement using spectroscopical stereo photogrammetry. *Optics Express,* 18**,** 26866-26871.

ZHAO, J., MA, J. Y., TIAN, J. W., MA, J., ZHANG, D. Z. & IEEE 2011. A Robust Method for Vector Field Learning with Application to Mismatch Removing. *2011 Ieee Conference on Computer Vision and Pattern Recognition.*

ZHU, S. & GAO, Y. 2010. Noncontact 3-D Coordinate Measurement of Cross-Cutting Feature Points on the Surface of a Large-Scale Workpiece Based on the Machine Vision Method. *IEEE Transactions on Instrumentation and Measurement,* 59**,** 1874-1887.